The IRM Quarterly
Fall 2020, Vol. 30 No. 3
ISSN: 2152-1972

Inside...

Practical Magnetism IV: feats and challenges in quantifying hematite with magnetic methods

Dario Bilardello
Institute for Rock Magnetism, University of Minnesota, Minneapolis, MN, USA
dario@umn.edu

Andrew P. Roberts
Research School of Earth Sciences, Australian National University,
Canberra, ACT 2601, Australia
andrew.roberts@anu.edu.au

Owing to its stable magnetization over geologic time scales, hematite is an important mineral for many magnetic applications, particularly for paleomagnetism (e.g. Butler, 1992) and environmental magnetism, including the study of soils (e.g. Heller & Liu, 1982, 1984; Maxbauer et al., 2016a; Schwertmann, 1985). Despite its favorable magnetic properties, hematite's weak spontaneous magnetization at room temperature (M_s = ~0.4 Am^2 kg^{-1}), which is similar to that of goethite (M_s = ~0.5 Am^2 kg^{-1}), but much weaker than magnetite (M_s = 92 Am^2 kg^{-1}), makes its magnetic quantification challenging. Even when small amounts of magnetite co-occur with hematite, its ~ ×230 stronger magnetization can overwhelm, if not effectively mask, the magnetic contribution of hematite (e.g. Dekkers, 1990; Frank & Nowaczyk, 2008). The weak spontaneous magnetization of hematite also belies its environmental importance because its mass far exceeds that of magnetite in many natural environments. Likewise, remanences of interest need not be the strongest, or carried by the most abundant phase. Identification, isolation, and quantification of the contributions to the bulk remanence, thus, become paramount to many applications.

In a recent article published in the open access journal *Geoscience Letters*, Roberts et al. (2020) outlined the main magnetic parameters used to quantify relative, absolute, or partial hematite contributions to the remanence to evaluate their limitations and effectiveness.

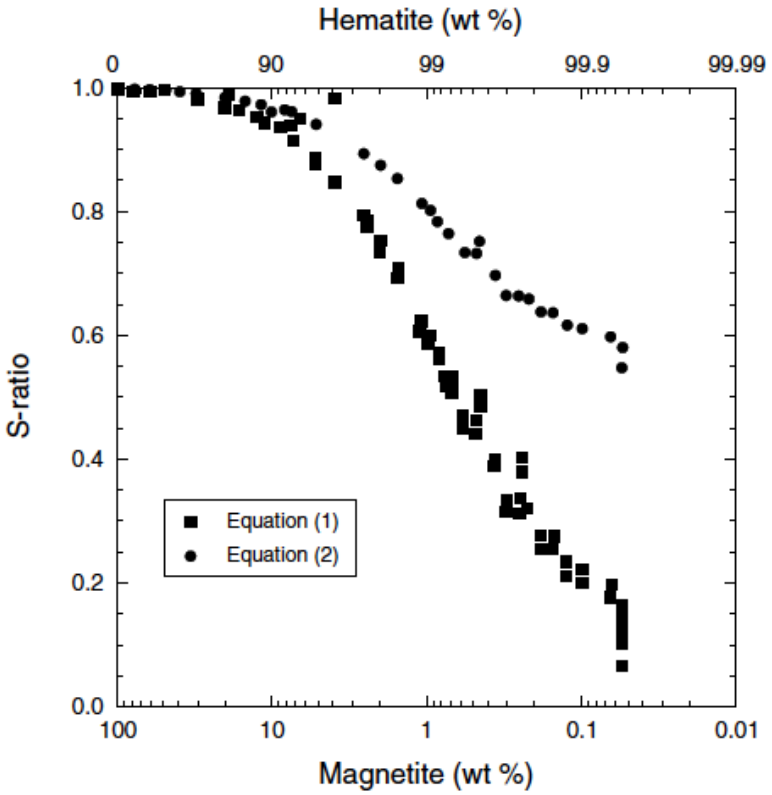

Figure 1. S-ratio variations for known mixing percentages of hematite (upper axis) and magnetite (lower axis) from synthetic powders. Values are compared for two versions of the S-ratio ("equation (1)" (Stober & Thompson, 1979) and "equation (2)" (Bloemendal et al., 1992)) with saturating fields of 1 and 2 T (not distinguished in the figure) and a 300 mT cut-off field (Redrawn by Roberts et al. (2020) from Frank and Nowaczyk (2008)).

Given the importance of the topic, we thought it useful to re-purpose these ideas here, often verbatim -no reason to reinvent the wheel- with permission from the authors and publisher, and with minor additions.

The observation

Roberts et al. (2020) reviewed the main magnetic proxies used to estimate the relative or absolute concentration of sedimentary hematite or its coercivity variations. These are: the S-ratio; the 'hard' isothermal remanent magnetization (HIRM); alternating field (AF) demagnetization

cont'd. on pg. 8...

The State of the Lab:

an update on the Visiting Fellowship program and other activities.

After the initial reopening of the lab in late May, the IRM has resumed essential research, allowing approved graduate students and researchers from the University of Minnesota to use the facilities, all while under strict safety protocols.

Since our reopening, we have been striving to serve the needs of the rock magnetic and paleomagnetic community to the greatest extent possible. In August, the IRM started "curbside service" where IRM staff began performing measurements on behalf of the 2020 Visiting Fellows who were willing to mail us their samples in lieu of visiting in-person. Due to strict limitations on the number of people simultaneously allowed in the lab and the inability to use our office spaces, we have focused on the most automated measurements possible, including low-temperature magnetometry experiments on the MPMSs, high-temperature susceptibility measurements on the AGICO KLY-2 Kappabridge, and excitingly, sequences of hysteresis loops, backfield demagnetization curves and FORC measurements, at room and variable temperatures, all of which can be programmed (and automated) on the new Lake Shore 8600 VSM, which arrived in late 2019.

More recently, we have begun collecting measurements for colleagues outside of our Visiting Fellowship program at the rates specified on our website (www.irm.umn.edu). We take this opportunity to advertise this measurement opportunity to all members of our community, but especially to those students and early career scientists who need data in a timely manner to push their research forward.

The University of Minnesota is now beginning to allow external visitors, provided that they follow strict health and safety protocols. However, it is likely that our visitor policies may change as the global COVID-19 situation continues to evolve (e.g., at the time of writing cases in Minnesota are rising faster than a Hopkinson peak). However, for the time being we are pleased to be scheduling in-person visits for awarded Visiting Fellows and external visitors alike.

It has been a very busy summer for all of us at the IRM! We have shut down and re-started the entire lab over the course of a few months with all the unexpected hiccups that goes with it. We have tried to support our community's research in all possible ways. We have also worked hard to install a new MPMS-3 system with remote guidance from Quantum Design, which will offer a number of tantalizing new measurement capabilities that we hope many of you will want to explore for your own research.

It has likely been a challenging year for all of you as well. We are all looking forward to a time when we can push forward with our research at a brisker, more 'normal' pace. Along these lines, we encourage you to contact us regarding visiting the lab, both formally or informally, or sending us your samples, and we will be happy to discuss any research needs you may have.

We wish you all the best and hope you are all staying safe and healthy!

Hope to see you soon,
The Institute for Rock Magnetism

Current Articles

A list of current research articles dealing with various topics in the physics and chemistry of magnetism is a regular feature of the IRM Quarterly. Articles published in familiar geology and geophysics journals are included; special emphasis is given to current articles from physics, chemistry, and materials-science journals. Most are taken from ISI Web of Knowledge, after which they are subjected to Procrustean culling for this newsletter. An extensive reference list of articles (primarily about rock magnetism, the physics and chemistry of magnetism, and some paleomagnetism) is continually updated at the IRM. This list, with more than 10,000 references, is available free of charge. Your contributions both to the list and to the Current Articles section of the IRM Quarterly are always welcome.

Aeromagnetism

Drenth, B. J., A. K. Souders, K. J. Schulz, J. M. Feinberg, R. R. Anderson, V. W. Chandler, W. F. Cannon, and R. J. Clark (2020), Evidence for a concealed Midcontinent Rift-related northeast Iowa intrusive complex, Precambrian Research, 347, doi:10.1016/j.precamres.2020.105845.

Archaeomagnetism

Herrero-Bervera, E., S. Athens, E. Tema, L. M. A. Valdivia, P. Camps, and A. R. Trejo (2020), First archaeointensity results from Ecuador with rock magnetic analyses and 14C dates to constrain the geomagnetic field evolution in South America: Enhancing the knowledge of geomagnetic field intensity, Journal of South American Earth Sciences, 103, doi:10.1016/j.jsames.2020.102733.

Lopez-Sanchez, J., et al. (2020), Further progress in the study of epsilon iron oxide in archaeological baked clays, Physics of the Earth and Planetary Interiors, 307, doi:10.1016/j.pepi.2020.106554.

Ozán, I. L., Orgeira, M. J., Buscaglia, S., Bianchi Villelli, M., Vásquez, C. A., Cieplicki, A., Naselli, M. (2020), Sediments vs. Historical narratives: The use of soil magnetic properties to evaluate the existence of a historical fire in an 18th century Spanish fort (Patagonia, Argentina), Journal of Archaeological Science: Reports, 34 A, doi:10.1016/j.jasrep.2020.102577.

Environmental Magnetism and Biomagnetism

Achilles, C. N., et al. (2020), Evidence for Multiple Diagenetic Episodes in Ancient Fluvial-Lacustrine Sedimentary Rocks in Gale Crater, Mars, Journal of Geophysical Research-Planets, 125(8), doi:10.1029/2019je006295.

Albuquerque, M. F. D., A. M. C. Horbe, and M. Danisik (2020), Episodic weathering in Southwestern Amazonia based on (U-Th)/He dating of Fe and Mn lateritic duricrust, Chemical Geology, 553, doi:10.1016/j.chemgeo.2020.119792.

Amiel, N., R. Shaar, and O. Sivan (2020), The Effect of Early Diagenesis in Methanic Sediments on Sedimentary Magnetic Properties: Case Study From the SE Mediterranean Continental Shelf, Frontiers in Earth Science, 8, doi:10.3389/feart.2020.00283.

Balescu, S., D. Jordanova, L. F. Brisson, F. Hardy, S. Huot, and M. Lamothe (2020), Luminescence chronology of the northeastern Bulgarian loess-paleosol sequences (Viatovo and Kaolinovo), Quaternary International, 552, 15-24, doi:10.1016/j.quaint.2019.04.020.

Bauer, K. W., et al. (2020), Magnetite biomineralization in ferruginous waters and early Earth evolution, Earth and Plan-

etary Science Letters, 549, doi:10.1016/j.epsl.2020.116495.
Bilardello, D., S. K. Banerjee, M. W. R. Volk, J. A. Soltis, and R. L. Penn (2020), Simulation of Natural Iron Oxide Alteration in Soil: Conversion of Synthetic Ferrihydrite to Hematite Without Artificial Dopants, Observed With Magnetic Methods, Geochemistry Geophysics Geosystems, 21(7), doi:10.1029/2020gc009037.
Bosq, M., et al. (2020), Chronostratigraphy of two Late Pleistocene loess-palaeosol sequences in the Rhone Valley (southeast France), Quaternary Science Reviews, 245, doi:10.1016/j.quascirev.2020.106473.
Cheng, L. Q., Y. G. Song, H. Y. Sun, B. Bradak, R. Orozbaev, X. L. Zong, and H. F. Liu (2020), Pronounced changes in paleo-wind direction and dust sources during MIS3b recorded in the Tacheng loess, northwest China, Quaternary International, 552, 122-134, doi:10.1016/j.quaint.2019.05.002.
Francke, A., A. Dosseto, J. Just, B. Wagner, and B. G. Jones (2020), Assessment of the controls on (U-234/U-238) activity ratios recorded in detrital lacustrine sediments, Chemical Geology, 550, doi:10.1016/j.chemgeo.2020.119698.
Jelavic, S., A. C. Mitchell, and K. K. Sand (2020), Fate of organic compounds during transformation of ferrihydrite in iron formations, Geochemical Perspectives Letters, 15, 25-29, doi:10.7185/geochemlet.2030.
Johansson, F. E., J. Bakke, E. N. Storen, O. Paasche, K. Engeland, and F. Arnaud (2020), Lake Sediments Reveal Large Variations in Flood Frequency Over the Last 6,500 Years in South-Western Norway, Frontiers in Earth Science, 8, doi:10.3389/feart.2020.00239.
Kameo, K., Y. Kubota, Y. Haneda, Y. Suganuma, and M. Okada (2020), Calcareous nannofossil biostratigraphy of the Lower-Middle Pleistocene boundary of the GSSP, Chiba composite section in the Kokumoto Formation, Kazusa Group, central Japan, and implications for sea-surface environmental changes, Progress in Earth and Planetary Science, 7(1), doi:10.1186/s40645-020-00355-x.
Keating, K., D. O. Walsh, and E. Grunewald (2020), The effect of magnetic susceptibility and magnetic field strength on porosity estimates determined from low-field nuclear magnetic resonance, Journal of Applied Geophysics, 179, doi:10.1016/j.jappgeo.2020.104096.
Kenis, P., J. Skurzynski, Z. Jary, and R. Kubik (2020), A new methodological approach (QEMSCAN (R)) in the mineralogical study of Polish loess: Guidelines for further research, Open Geosciences, 12(1), 342-353, doi:10.1515/geo-2020-0138.
Kong, X. H., W. J. Zhou, J. W. Beck, F. Xian, X. K. Qiang, H. Ao, Z. K. Wu, and Z. S. An (2020), Loess magnetic susceptibility flux: A new proxy of East Asian monsoon precipitation, Journal of Asian Earth Sciences, 201, doi:10.1016/j.jseaes.2020.104489.
Kosareva, L. R., V. P. Shcherbakov, D. K. Nurgaliev, N. G. Nurgalieva, N. K. Sycheva, V. V. Antonenko, D. M. Kuzina, and V. G. Evtyugin (2020), Periodization of Holocene Climatic Cycles Based on Synchronous Variations in the Magnetic and Geochemical Parameters of the Sediments of Lake Bolshoe Yarovoe (Southwestern Siberia), Russian Geology and Geophysics, 61(7), 723-737, doi:10.15372/rgg2019148.
Lee, S., S. Kim, H. Kim, Y. Seo, Y. Ha, R. Ha, and Y. Yu (2020), Tracing of traffic-related pollution using magnetic properties of topsoils in Daejeon, Korea, Environmental Earth Sciences, 79(20), doi:10.1007/s12665-020-09223-9.
Li, G. H., D. S. Xia, H. Lu, Y. J. Wang, J. Jia, X. B. Liu, and X. Q. Yang (2020a), Magnetic, granulometric and geochemical characterizations of loess sections in the eastern Arid Central Asia: Implication for paleoenvironmental interpretations, Quaternary International, 552, 135-147, doi:10.1016/j.quaint.2020.01.003.
Li, J. H., et al. (2020b), Bullet-Shaped Magnetite Biomineralization Within a Magnetotactic Deltaproteobacterium: Implications for Magnetofossil Identification, Journal of Geophysical Research-Biogeosciences, 125(7), doi:10.1029/2020jg005680.
Li, M. K., S. Y. Zhu, T. P. Ouyang, J. H. Tang, and C. J. He (2020c), Magnetic fingerprints of surface sediment in the Bohai Sea, China, Marine Geology, 427, doi:10.1016/j.margeo.2020.106226.
Li, Y., G. L. Wei, X. L. Liang, C. H. Zhang, J. X. Zhu, and Y. Arai (2020f), Metal Substitution-Induced Reducing Capacity of Magnetite Coupled with Aqueous Fe(II), Acs Earth and Space Chemistry, 4(6), 905-911, doi:10.1021/acsearthspacechem.0c00089.
Lozhkin, A., M. Cherepanova, P. Anderson, P. Minyuk, B. Finney, A. Pakhomov, T. Brown, J. Korzun, and V. Tsigankova (2020), Late Holocene history of Tokotan Lake (Kuril Archipelago, Russian Far East): The use of lacustrine records for paleoclimatic reconstructions from geologically dynamic settings, Quaternary International, 553, 104-117, doi:10.1016/j.quaint.2020.05.023.
Mendez, J. C., and T. Hiemstra (2020), High and low affinity sites of ferrihydrite for metal ion adsorption: Data and modeling of the alkaline-earth ions Be, Mg, Ca, Sr, Ba, and Ra, Geochimica Et Cosmochimica Acta, 286, 289-305, doi:10.1016/j.gca.2020.07.032.
Messaoud, J. H., N. Thibault, C. Yaich, J. Monkenbusch, H. Omar, H. F. Ben Jemai, and D. K. Watkins (2020), The Eocene-Oligocene Transition in the South-Western Neo-Tethys (Tunisia): Astronomical Calibration and Paleoenvironmental Changes, Paleoceanography and Paleoclimatology, 35(8), doi:10.1029/2020pa003887.
Micallef, A., A. Georgiopoulou, A. Green, and V. Maselli (2020), Impact of sea-level fluctuations on the sedimentation patterns of the SE African margin: implications for slope instability, in Subaqueous Mass Movements and Their Consequences: Advances in Process Understanding, Monitoring and Hazard Assessments, edited by A. Georgiopoulou, L. A. Amy, S. Benetti, J. D. Chaytor, M. A. Clare, D. Gamboa, P. D. W. Haughton, J. Moernaut and J. J. Mountjoy, pp. 267-276, doi:10.1144/sp500-2019-172.
Newton, K. C., and S. M. Kajiura (2020), The yellow stingray (Urobatis jamaicensis) can discriminate the geomagnetic cues necessary for a bicoordinate magnetic map, Marine Biology, 167(10), doi:10.1007/s00227-020-03763-1.
O'Connor, J. E., V. R. Baker, R. B. Waitt, L. N. Smith, C. M. Cannon, D. L. George, and R. P. Denlinger (2020), The Missoula and Bonneville floods-A review of ice-age megafloods in the Columbia River basin, Earth-Science Reviews, 208, doi:10.1016/j.earscirev.2020.103181.
Oldknow, C. J., F. Oldfield, A. S. Carr, J. M. Hooke, A. Biggin, J. F. Boyle, A. Hunt, and Z. Shen (2020), Palustrine wetland formation during the MIS 3 interstadial: Implications for preserved alluvial records in the South African Karoo, Sedimentary Geology, 405, doi:10.1016/j.sedgeo.2020.105698.
Pfeifer, L. S., L. Hinnov, C. Zeeden, C. Rolf, C. Laag, and G. S. Soreghan (2020), Rock Magnetic Cyclostratigraphy of Permian Loess in Eastern Equatorial Pangea (Salagou Formation, South-Central France), Frontiers in Earth Science, 8, doi:10.3389/feart.2020.00241.
Roban, R. D., et al. (2020), Lower Cretaceous Provenance and Sedimentary Deposition in the Eastern Carpathians: Inferences for the Evolution of the Subducted Oceanic Domain and its European Passive Continental Margin, Tectonics, 39(7), doi:10.1029/2019tc005780.

Rousseau, M., F. Demory, C. Miramont, E. Brisset, F. Guiter, P. Sabatier, and P. Sorrel (2020), Palaeoenvironmental change and glacier fluctuations in the high Tian Shan Mountains during the last millennium based on sediments from Lake Ala Kol, Kyrgyzstan, Palaeogeography Palaeoclimatology Palaeoecology, 558, doi:10.1016/j.palaeo.2020.109987.

Schwamborn, G., et al. (2020), Sediment history mirrors Pleistocene aridification in the Gobi Desert (Ejina Basin, NW China), Solid Earth, 11(4), 1375-1398, doi:10.5194/se-11-1375-2020.

Sharifigarmdareh, J., F. Khormali, S. Scheidt, C. Rolf, M. Kehl, and M. Frechen (2020), Investigating soil magnetic properties with pedogenic variation along a precipitation gradient in loess-derived soils of the Golestan province, northern Iran, Quaternary International, 552, 100-110, doi:10.1016/j.quaint.2019.11.022.

Sharma, S., R. Agnihotri, A. K. Pokharia, B. Phartiyal, S. Bajpai, P. C. Pande, S. K. Manjul, A. Manzul, C. Maharana, and S. Ojha (2020), Environmental magnetic, Geochemical and Sulfur isotopic imprints of an Indus archaeological site 4MSR from western India (Rajasthan): Implications to the Indus industrial (metallurgical) activities, Quaternary International, 550, 74-84, doi:10.1016/j.quaint.2020.03.038.

Shi, Y. H., X. G. Mao, X. M. Liu, and B. Lu (2020b), Magnetic characteristics and environmental responses of vertical zonal soils in the subtropical mountains, Chinese Journal of Geophysics-Chinese Edition, 63(9), 3420-3430, doi:10.6038/cjg2020N0351.

Shilling, A. M., et al. (2020), Biogeochemical evidence from OGCP Core 2A sediments for environmental changes preceding deposition of Tuff IB and climatic transitions in Upper Bed I of the Olduvai Basin, Palaeogeography Palaeoclimatology Palaeoecology, 555, doi:10.1016/j.palaeo.2020.109824.

Shin, J. Y., S. Kim, X. Zhao, K. C. Yoo, Y. Yu, J. I. Lee, M. K. Lee, and H. I. Yoon (2020a), Particle-size dependent magnetic properties of Scotia Sea sediments since the Last Glacial Maximum: Glacial ice-sheet discharge controlling magnetic proxies, Palaeogeography Palaeoclimatology Palaeoecology, 557, doi:10.1016/j.palaeo.2020.109906.

Shin, J. Y., W. Kim, and K. Hyeong (2020b), High Potency of Volcanic Contribution to the similar to 400 kyr Sedimentary Magnetic Record in the Northwest Pacific, Frontiers in Earth Science, 8, doi:10.3389/feart.2020.00300.

Szeberenyi, J., J. Kovacs, B. Bradak, G. Barta, D. Csonka, A. Medvedova, P. Rostinsky, K. Kiss, and G. Varga (2020), Experiencing new perspectives in the application of reflectance spectroscopy in loess research, Quaternary International, 552, 36-49, doi:10.1016/j.quaint.2019.09.035.

Tang, D. J., J. B. Ma, X. Y. Shi, M. Lechte, and X. Q. Zhou (2020), The formation of marine red beds and iron cycling on the Mesoproterozoic North China Platform, American Mineralogist, 105(9), 1412-1423, doi:10.2138/am-2020-7406.

Tauxe, L., and S. J. Feakins (2020), A Reassessment of the Chronostratigraphy of Late Miocene C-3-C-4 Transitions, Paleoceanography and Paleoclimatology, 35(7), doi:10.1029/2020pa003857.

Teixeira, M., et al. (2020), The Late Pleistocene-Holocene sedimentary evolution of the Sines Contourite Drift (SW Portuguese Margin): A multiproxy approach, Sedimentary Geology, 407, doi:10.1016/j.sedgeo.2020.105737.

Tian, C. J., T. P. Ouyang, M. K. Li, J. L. Zhang, S. S. Peng, Z. Y. Zhu, X. C. Peng, Q. Hu, Y. Qiu, and H. J. Chen (2020), Magnetic investigation of surface sediments of the northwestern South China Sea: Implication for sediment provenance and transportation, Journal of Asian Earth Sciences, 202, doi:10.1016/j.jseaes.2020.104530.

Wang, F., W. G. Zhang, X. M. Nian, A. P. Roberts, X. Zhao, Y. Shang, C. Ge, and Y. Dong (2020a), Magnetic evidence for Yellow River sediment in the late Holocene deposit of the Yangtze River Delta, China, Marine Geology, 427, doi:10.1016/j.margeo.2020.106274.

Wang, Q. S., Y. G. Song, and Y. Li (2020c), Clay mineralogy of the upper Miocene-Pliocene red clay from the central Chinese Loess Plateau and its paleoclimate implications, Quaternary International, 552, 148-154, doi:10.1016/j.quaint.2019.11.039.

Wasiljeff, J., A. Kaakinen, J. M. Salminen, and Z. Q. Zhang (2020), Magnetostratigraphic constraints on the fossiliferous Ulantatal sequence in Inner Mongolia, China: Implications for Asian aridification and faunal turnover before the Eocene-Oligocene boundary, Earth and Planetary Science Letters, 536, doi:10.1016/j.epsl.2020.116125.

Xue, W. P., H. L. Jin, B. Liu, L. Y. Sun, and Z. Y. Liu (2020), History of moisture change indicated by aeolian deposit in the Horqin sandy land, Northeastern China since the Last Glacial Maximum, Quaternary International, 547, 50-62, doi:10.1016/j.quaint.2019.12.022.

Zan, J. B., X. M. Fang, J. Kang, X. J. Li, and M. D. Yan (2020), Spatial and altitudinal variations in the magnetic properties of eolian deposits in the northern Tibetan Plateau and its adjacent regions: Implications for delineating the climatic boundary, Earth-Science Reviews, 208, doi:10.1016/j.earscirev.2020.103271.

Zhang, Y., A. R. Muxworthy, D. Jia, G. Q. Wei, B. Xia, B. Wen, M. M. Wang, W. L. Liu, and M. J. Brzozowski (2019), Identifying and Dating the Destruction of Hydrocarbon Reservoirs Using Secondary Chemical Remanent Magnetization, Geophysical Research Letters, 46(20), 11100-11108, doi:10.1029/2019gl084812.

Extraterrestrial Magnetism

Blukis, R., B. Pfau, C. M. Gunther, P. Hessing, S. Eisebitt, J. Einsle, and R. J. Harrison (2020), Nanoscale Imaging of High-Field Magnetic Hysteresis in Meteoritic Metal Using X-Ray Holography, Geochemistry Geophysics Geosystems, 21(8), doi:10.1029/2020gc009044.

Rampe, E. B., et al. (2020), Mineralogy of Vera Rubin Ridge From the Mars Science Laboratory CheMin Instrument, Journal of Geophysical Research-Planets, 125(9), doi:10.1029/2019je006306.

Ravat, D., M. E. Purucker, and N. Olsen (2020), Lunar Magnetic Field Models From Lunar Prospector and SELENE/Kaguya Along-Track Magnetic Field Gradients, Journal of Geophysical Research-Planets, 125(7), doi:10.1029/2019je006187.

Stys, C., and M. Dumberry (2020), A Past Lunar Dynamo Thermally Driven by the Precession of Its Inner Core, Journal of Geophysical Research-Planets, 125(7), doi:10.1029/2020je006396.

Fundamental Rock Magnetism and direct Applications

Ahmadzadeh, M., A. Scrimshire, L. Mottram, M. C. Stennett, N. C. Hyatt, P. A. Bingham, and J. S. McCloy (2020), Structure of NaFeSiO4, NaFeSi2O6, and NaFeSi3O8 glasses and glass-ceramics, American Mineralogist, 105(9), 1375-1384, doi:10.2138/am-2020-7285.

Chen, H. W., et al. (2020a), A new hydrous iron oxide phase stable at mid-mantle pressures, Earth and Planetary Science Letters, 550, doi:10.1016/j.epsl.2020.116551.

Cruz, C., H. Sant'ovaia, and F. Noronha (2020), Magnetic mineralogy of Variscan granites from northern Portugal: an

approach to their petrogenesis and metallogenic potential, Geologica Acta, 18, doi:10.1344/GeologicaActa2020.18.5.
Duan, Z. Q., Q. S. Liu, H. F. Qin, X. X. Zhao, and X. Gao (2020), Behavior of Greigite-Bearing Marine Sediments During AF and Thermal Demagnetization and Its Significance, Geochemistry Geophysics Geosystems, 21(7), doi:10.1029/2019gc008635.
Haines, C. R. S., G. I. Lampronti, W. T. Klooster, S. J. Coles, S. E. Dutton, and M. A. Carpenter (2020), Morin-type transition in 5C pyrrhotite, American Mineralogist, 105(9), 1404-1411, doi:10.2138/am-2020-7266.
Horng, C. S., A. P. Roberts, Y. H. Chen, K. S. Shea, K. H. Chen, C. H. Lin, X. Zhao, and C. K. Chang (2020), Magnetic Properties of Sedimentary Smythite (Fe9S11), Journal of Geophysical Research-Solid Earth, 125(6), doi:10.1029/2019jb018812.
Li, Z. Y., B. M. Moskowitz, J. P. Zheng, Q. Xiong, X. Zhou, J. S. Yang, Y. W. Zhang, and Q. S. Liu (2020g), Petromagnetic Characteristics of Serpentinization and Magnetite Formation at the Zedang Ophiolite in Southern Tibet, Journal of Geophysical Research-Solid Earth, 125(9), doi:10.1029/2020jb019696.
Liu, Z. B., J. C. Li, T. Zhao, Y. Song, G. L. Yuan, Y. Lin, and H. S. Shao (2020), Serpentinisation and magnetite formation in the Angwu ultramafic rocks from the central Bangong-Nujiang suture zone, Tibetan Plateau, Geological Journal, 55(2), 1283-1299, doi:10.1002/gj.3496.
Yamazaki, T., W. Fu, T. Shimono, and Y. Usui (2020), Unmixing biogenic and terrigenous magnetic mineral components in red clay of the Pacific Ocean using principal component analyses of first-order reversal curve diagrams and paleoenvironmental implications, Earth Planets and Space, 72(1), doi:10.1186/s40623-020-01248-5.

Paleointensity, Geomagnetism and Records of the Geomagnetic Field

Bono, R. K., A. J. Biggin, R. Holme, C. J. Davies, D. G. Meduri, and J. Bestard (2020), Covariant Giant Gaussian Process Models With Improved Reproduction of Palaeosecular Variation, Geochemistry Geophysics Geosystems, 21(8), doi:10.1029/2020gc008960.
Bouffard, M., M. Landeau, and A. Goument (2020), Convective Erosion of a Primordial Stratification Atop Earth's Core, Geophysical Research Letters, 47(14), doi:10.1029/2020gl087109.
Haneda, Y., M. Okada, Y. Suganuma, and T. Kitamura (2020), A full sequence of the Matuyama-Brunhes geomagnetic reversal in the Chiba composite section, Central Japan, Progress in Earth and Planetary Science, 7(1), doi:10.1186/s40645-020-00354-y.
Morales, J., N. Perez-Rodriguez, A. Goguitchaichvili, and M. Cervantes-Solano (2020), A multimethod paleointensity approach applied to the historical Xitle lava flows (Central Mexico): towards the accurate paleointensity determination, Earth Planets and Space, 72(1), doi:10.1186/s40623-020-01232-z.
Munch, F. D., A. V. Grayver, M. Guzavina, A. V. Kuvshinov, and A. Khan (2020), Joint Inversion of Daily and Long-Period Geomagnetic Transfer Functions Reveals Lateral Variations in Mantle Water Content, Geophysical Research Letters, 47(10), doi:10.1029/2020gl087222.
Nakagawa, T. (2020), A coupled core-mantle evolution: review and future prospects, Progress in Earth and Planetary Science, 7(1), doi:10.1186/s40645-020-00374-8.
Ringler, A. T., R. E. Anthony, D. C. Wilson, A. C. Claycomb, and J. Spritzer (2020), Magnetic Field Variations in Alaska: Recording Space Weather Events on Seismic Stations in Alaska, Bulletin of the Seismological Society of America, 110(5), 2530-2540, doi:10.1785/0120200019.
Simon, Q., N. Thouveny, D. L. Bourles, J. P. Valet, and F. Bassinot (2020), Cosmogenic Be-10 production records reveal dynamics of geomagnetic dipole moment (GDM) over the Laschamp excursion (20-60 ka), Earth and Planetary Science Letters, 550, doi:10.1016/j.epsl.2020.116547.
Wang, H. S., X. Xu, Q. S. Liu, Y. Zhong, T. Chen, X. K. Qiang, Y. M. Chou, and X. Q. Yang (2020b), Geomagnetic paleointensity and its geodynamic significance for the last 40 ka recorded in the northwestern sub-sea basin of the South China Sea, Chinese Journal of Geophysics-Chinese Edition, 63(7), 2671-2681, doi:10.6038/cjg2020N0353.

Magnetic Fabrics and Anisotropy

Boiron, T., C. Aubourg, P. A. Grignard, and J. P. Callot (2020), The clay fabric of shales is a strain gauge, Journal of Structural Geology, 138, doi:10.1016/j.jsg.2020.104130.
Goncalves, A., H. Sant'Ovaia, M. D. Ribeiro, and F. Noronha (2020), The Esmolfe-Matanca granite (Penalva do Castelo, central Portugal): A keystone to understand the ascent and emplacement of magmas under low tectonic stress, Journal of Structural Geology, 139, doi:10.1016/j.jsg.2020.104143.
Hrouda, F., J. Jezek, and M. Chadima (2020), Anisotropy of out-of-phase magnetic susceptibility as a potential tool for distinguishing geologically and physically controlled inverse magnetic fabrics in volcanic dykes, Physics of the Earth and Planetary Interiors, 307, doi:10.1016/j.pepi.2020.106551.
Qiu, H. B., W. Lin, M. Faure, Y. Chen, L. T. Meng, J. P. Zeng, Z. H. Ren, Y. Wang, and Q. L. Li (2020), Late Triassic extensional tectonics in the northern North China Craton, insights from a multidisciplinary study of the Wangtufang pluton, Journal of Asian Earth Sciences, 200, doi:10.1016/j.jseaes.2020.104462.
Ramesh, B. N., E. Nagaraju, V. Parashuramulu, and M. Venkateshwarlu (2020), Preliminary anisotropy of magnetic susceptibility studies on 2367 Ma Bangalore-Karimnagar giant dyke swarm, southern India: Implications for magma flow, Physics of the Earth and Planetary Interiors, 306, doi:10.1016/j.pepi.2020.106540.
Satolli, S., C. R. Test, D. Staneczek, E. Zanella, F. Calamita, and E. Tema (2020), Magnetic fabric in carbonatic rocks from thrust shear zones: A study from the Northern Apennines (Italy), Tectonophysics, 791, doi:10.1016/j.tecto.2020.228573.

Magnetic Microscopy

Fu, R. R., E. A. Lima, M. W. R. Volk, and R. Trubko (2020), High-Sensitivity Moment Magnetometry With the Quantum Diamond Microscope, Geochemistry Geophysics Geosystems, 21(8), doi:10.1029/2020gc009147.

Mineralogy and Petrology

Ageeva, O., G. Bian, G. Habler, A. Pertsev, and R. Abart (2020), Crystallographic and shape orientations of magnetite micro-inclusions in plagioclase, Contributions to Mineralogy and Petrology, 175(10), doi:10.1007/s00410-020-01735-8.
Campione, M., M. La Fortezza, M. Alvaro, M. Scambelluri, and N. Malaspina (2020), Commensurate Growth of Magnetite Microinclusions in Olivine under Mantle Conditions, Acs Earth and Space Chemistry, 4(6), 825-830, doi:10.1021/acsearthspacechem.0c00026.
Cooperdock, E. H. G., D. F. Stockli, P. B. Kelemen, and J. C. de Obeso (2020), Timing of Magnetite Growth Associated With Peridotite-Hosted Carbonate Veins in the SE Samail

Ophiolite, Wadi Fins, Oman, Journal of Geophysical Research-Solid Earth, 125(5), doi:10.1029/2019jb018632.

Paleomagnetism

Bian, W. W., et al. (2020), Paleomagnetism of the Late Cretaceous Red Beds From the Far Western Lhasa Terrane: Inclination Discrepancy and Tectonic Implications, Tectonics, 39(8), doi:10.1029/2020tc006280.

Cao, Y., et al. (2020), Paleomagnetism and U-Pb Geochronology of Early Cretaceous Volcanic Rocks from the Qiangtang Block, Tibetan Plateau: Implications for the Qiangtang-Lhasa Collision, Tectonophysics, 789, doi:10.1016/j.tecto.2020.228500.

Chen, Z. L., F. Yuan, J. Z. Zhang, S. H. Shen, X. H. Li, X. L. Li, M. Huang, and S. M. Jowitt (2020b), Paleomagnetic evidence for the Gothenburg geomagnetic excursion during the Pleistocene-Holocene transition recorded in the Paleo-Danyang Lake, eastern China, Journal of Asian Earth Sciences, 201, doi:10.1016/j.jseaes.2019.104140.

Ge, K. P., J. H. Xie, Y. G. Ying, D. D. Qiu, Y. Q. Wang, and J. Z. Deng (2020), A new paleomagnetic method of borehole core reorientation and its preliminary applications in reorientation of cores of uranium deposits in southern China, Chinese Journal of Geophysics-Chinese Edition, 63(8), 3037-3049, doi:10.6038/cjg2020O0108.

Heij, G. W., and R. D. Elmore (2020), Burial Diagenesis and Tectonism Inferred From Paleomagnetism and Magnetic Fabrics in the Wolfcamp Shale, Midland Basin, Texas, USA, Journal of Geophysical Research-Solid Earth, 125(5), doi:10.1029/2019jb019046.

Heslop, D., and A. P. Roberts (2020), Uncertainty Propagation in Hierarchical Paleomagnetic Reconstructions, Journal of Geophysical Research-Solid Earth, 125(6), doi:10.1029/2020jb019488.

Izquierdo-Llavall, E., A. Menant, C. Aubourg, J. P. Callot, G. Hoareau, P. Camps, E. Pere, and A. Lahfid (2020), Preorogenic Folds and Syn-Orogenic Basement Tilts in an Inverted Hyperextended Margin: The Northern Pyrenees Case Study, Tectonics, 39(7), doi:10.1029/2019tc005719.

Kapawar, M. R., and V. Mamilla (2020), Paleomagnetism and rock magnetism of early Cretaceous Rajmahal basalts, NE India: Implications for paleogeography of the Indian subcontinent and migration of the Kerguelen hotspot, Journal of Asian Earth Sciences, 201, doi:10.1016/j.jseaes.2020.104517.

Kirscher, U., H. Gevorgyan, K. Meliksetian, G. Navasardyan, E. Dallanave, C. Breitkreuz, and V. Bachtadse (2020), Pleistocene ignimbrites of western Armenia - Paleomagnetic and magnetic anisotropy constraints on flow direction and stratigraphy, Journal of Volcanology and Geothermal Research, 402, doi:10.1016/j.jvolgeores.2020.106982.

Knott, T. R., M. J. Branney, M. K. Reichow, D. R. Finn, S. Tapster, and R. S. Coe (2020), Discovery of two new super-eruptions from the Yellowstone hotspot track (USA): Is the Yellowstone hotspot waning?, Geology, 48(9), 934-938, doi:10.1130/g47384.1.

Li, S., Y. L. Li, X. D. Tan, J. Meng, Y. M. Shang, Y. S. Wei, and C. S. Wang (2020d), Paleomagnetism and microtextures reveal Neohimalayan deformation pattern in the northwestern Tethys Himalaya, Journal of Asian Earth Sciences, 202, doi:10.1016/j.jseaes.2020.104516.

Li, S., C. Q. Yin, C. Guilmette, and L. Ding (2020e), Reply to comment by LZ Shi et al. on "Birth and demise of the Bangong-Nujiang Tethyan Ocean: A review from the Gerze area of central Tibet", Earth-Science Reviews, 208, doi:10.1016/j.earscirev.2020.103213.

Meert, J. G., A. F. Pivarunas, D. A. D. Evans, S. A. Pisarevsky, L. J. Pesonen, Z. X. Li, S. K. Elming, S. R. Miller, S. H. Zhang, and J. M. Salminen (2020), The magnificent seven: A proposal for modest revision of the Van der Voo (1990) quality index, Tectonophysics, 790, doi:10.1016/j.tecto.2020.228549.

Meng, J., F. Lhuillier, C. S. Wang, H. Liu, B. Eid, and Y. L. Li (2020), Paleomagnetism of Paleocene-Maastrichtian (60-70 Ma) Lava Flows From Tian Shan (Central Asia): Directional Analysis and Paleointensities, Journal of Geophysical Research-Solid Earth, 125(9), doi:10.1029/2019jb018631.

Miki, M., H. Seki, Y. Yamamoto, C. Gouzu, H. Hyodo, K. Uno, and Y. Otofuji (2020), Paleomagnetism, paleointensity and geochronology of a Proterozoic dolerite dyke from southern West Greenland, Journal of Geodynamics, 139, doi:10.1016/j.jog.2020.101752.

Risica, G., A. Di Roberto, F. Speranza, P. Del Carlo, M. Pompilio, S. Meletlidis, and M. Rosi (2020), Refining the Holocene eruptive activity at Tenerife (Canary Islands): The contribution of palaeomagnetism, Journal of Volcanology and Geothermal Research, 401, doi:10.1016/j.jvolgeores.2020.106930.

Pivarunas, A. F., and J. G. Meert (2020), Intracratonic stability: A comparison of paleomagnetic data from the north and the south of Dharwar Craton, India, Precambrian Research, 348, doi:10.1016/j.precamres.2020.105858.

Puigdomenech, C., R. Somoza, A. Tomlinson, and E. M. Renda (2020), Paleomagnetic data from the Precordillera of northern Chile: A multiphase rotation history related to a multiphase deformational history, Tectonophysics, 791, doi:10.1016/j.tecto.2020.228569.

Robert, B., M. Domeier, and J. Jakob (2020), Iapetan Oceans: An analog of Tethys?, Geology, 48(9), 929-933, doi:10.1130/g47513.1.

Shi, L. Z., J. Y. Huang, and W. Chen (2020a), Birth and demise of the Bangong-Nujiang Tethyan Ocean: A review from the Gerze area of Central Tibet: Comment, Earth-Science Reviews, 208, doi:10.1016/j.earscirev.2020.103209.

Todrani, A., B. Zhang, F. Speranza, and S. Y. Chen (2020), Paleomagnetism of the Middle Cenozoic Mula Basin (East Tibet): Evidence for km-Scale Crustal Blocks Rotated by Midlower Crust Drag, Geochemistry Geophysics Geosystems, 21(9), doi:10.1029/2020gc009225.

Wei, B. T., et al. (2020), An Absolute Paleogeographic Positioning of the Early Permian Tarim Large Igneous Province, Journal of Geophysical Research-Solid Earth, 125(5), doi:10.1029/2019jb019111.

Williams-Jones, G., R. W. Barendregt, J. K. Russell, Y. Le Moigne, R. J. Enkin, and R. Gallo (2020), The age of the Tseax volcanic eruption, British Columbia, Canada, Canadian Journal of Earth Sciences, 57(10), 1238-1253, doi:10.1139/cjes-2019-0240.

Yan, Y. G., L. Duan, S. M. Liang, J. H. Wang, B. C. Huang, W. J. Zheng, and P. Z. Zhang (2020), Paleomagnetic Constraint on the Carboniferous Paleoposition of Indochina and Its Implications for the Evolution of Eastern Paleo-Tethys Ocean, Tectonics, 39(7), doi:10.1029/2020tc006168.

Yasuda, Y., E. Sato, and K. Suzuki-Kamata (2020), Paleomagnetic constraints on a time-stratigraphic framework for the evolution of Ohachidaira volcano and the summit caldera, central Hokkaido, Japan, Bulletin of Volcanology, 82(11), doi:10.1007/s00445-020-01403-6.

Yi, Z. Y., and J. G. Meert (2020), A Closure of the Mongol-Okhotsk Ocean by the Middle Jurassic: Reconciliation of Paleomagnetic and Geological Evidence, Geophysical Research Letters, 47(15), doi:10.1029/2020gl088235.

Zhang, W. L., X. M. Fang, T. Zhang, C. H. Song, and M. D.

Yan (2020), Eocene Rotation of the Northeastern Central Tibetan Plateau Indicating Stepwise Compressions and Eastward Extrusions, Geophysical Research Letters, 47(17), doi:10.1029/2020gl088989.

Zhang, Z. L., and J. M. Sun (2020), Cenozoic tectonic rotations in different parts of the NE Pamir: implications for the evolution of the arcuate orogen, International Journal of Earth Sciences, 109(6), 1921-1939, doi:10.1007/s00531-020-01880-2.

Stratigraphy

Dallanave, E., and L. Chang (2020), Early Eocene to early Miocene magnetostratigraphic framework for IODP Expedition 371 (Tasman Frontier Subduction Initiation and Paleogene Climate), Newsletters on Stratigraphy, 53(4), 365-387, doi:10.1127/nos/2019/0556.

Dallanave, E., P. Maurizot, C. Agnini, R. Sutherland, C. J. Hollis, J. Collot, G. R. Dickens, V. Bachtadse, D. Strogen, and H. E. G. Morgans (2020), Eocene (46-44 Ma) Onset of Australia-Pacific Plate Motion in the Southwest Pacific Inferred From Stratigraphy in New Caledonia and New Zealand, Geochemistry Geophysics Geosystems, 21(7), doi:10.1029/2019gc008699.

Du, W., Y. L. Ji, G. Chen, H. Wu, C. L. Gao, S. M. Li, and Y. Zhang (2020), Cyclostratigraphy and astronomical tuning during the Oligocene in the Jizhong Depression, Bohai Bay Basin, northeastern China, Palaeogeography Palaeoclimatology Palaeoecology, 554, doi:10.1016/j.palaeo.2020.109803.

Fendley, I. M., et al. (2020), No Cretaceous-Paleogene Boundary in Exposed Rajahmundry Traps: A Refined Chronology of the Longest Deccan Lava Flows From Ar-40/Ar-39 Dates, Magnetostratigraphy, and Biostratigraphy, Geochemistry Geophysics Geosystems, 21(9), doi:10.1029/2020gc009149.

Flynn, A. G., A. J. Davis, T. E. Williamson, M. Heizler, C. W. Fenley, C. E. Leslie, R. Secord, S. L. Brusatte, and D. J. Peppe (2020), Early Paleocene Magnetostratigraphy and Revised Biostratigraphy of the Ojo Alamo Sandstone and Lower Nacimiento Formation, San Juan Basin, New Mexico, USA, Geological Society of America Bulletin, 132(9-10), 2154-2174, doi:10.1130/b35481.1.

Frydenvang, J., et al. (2020), The Chemostratigraphy of the Murray Formation and Role of Diagenesis at Vera Rubin Ridge in Gale Crater, Mars, as Observed by the ChemCam Instrument, Journal of Geophysical Research-Planets, 125(9), doi:10.1029/2019je006320.

Gnibidenko, Z. N., O. B. Kuzmina, and A. V. Levicheva (2020), Regional Magnetostratigraphy of the Upper Cretaceous and the Cretaceous-Paleogene Boundary in Southern West Siberia as Applied to Complitation of the Cretaceous Magnetic-Polarity Scale, Russian Geology and Geophysics, 61(9), 1028-1035, doi:10.15372/rgg2019170.

Hu, X. Z., Y. Q. Zhang, Y. X. Li, S. X. Ma, and J. P. Li (2020), Post-orogenic tectonic evolution of the Qinling belt, central China: Insights from a magnetostratigraphic study of a Cretaceous intra-mountain basin sedimentary succession, Journal of Asian Earth Sciences, 202, doi:10.1016/j.jseaes.2020.104496.

Konishi, T., and M. Okada (2020), A paleomagnetic record of the early Matuyama chron including the Reunion subchron and the onset Olduvai boundary: High-resolution magnetostratigraphy and insights from transitional geomagnetic fields, Progress in Earth and Planetary Science, 7(1), doi:10.1186/s40645-020-00352-0.

Milanese, F. N., E. B. Olivero, S. P. Slotznick, T. S. Tobin, M. E. Raffi, S. M. Skinner, J. L. Kirschvink, and A. E. Rapalini (2020), Coniacian-Campanian magnetostratigraphy of the Marambio Group: The Santonian-Campanian boundary in the Antarctic Peninsula and the complete Upper Cretaceous - Lowermost Paleogene chronostratigraphical framework for the James Ross Basin, Palaeogeography Palaeoclimatology Palaeoecology, 555, doi:10.1016/j.palaeo.2020.109871.

Nitta, H., T. Saito, and Y. Shitaoka (2020), Recent eruption history inferred from eruption ages of the two latest lava flows using multi-dating at Yokodake Volcano, Japan, Earth Planets and Space, 72(1), doi:10.1186/s40623-020-01220-3.

Palcu, D. V., J. R. Muraszko, P. F. Jaqueto, and L. Jovane (2020), The Birth of a Connected South Atlantic Ocean: A Magnetostratigraphic Perspective, Frontiers in Earth Science, 8, doi:10.3389/feart.2020.00375.

Trifonov, V. G., et al. (2020), The Upper Pliocene - Quaternary geological history of the Shirak Basin (NE Turkey and NW Armenia) and estimation of the Quaternary uplift of Lesser Caucasus, Quaternary International, 546, 229-244, doi:10.1016/j.quaint.2019.11.004.

Xuan, C., Y. X. Jin, S. Sugisaki, Y. Satoguchi, and Y. Nagahashi (2020), Integrated Pliocene-Pleistocene magnetostratigraphy and tephrostratigraphy of deep-sea sediments at IODP Site U1424 (Yamato Basin, Japan Sea), Progress in Earth and Planetary Science, 7(1), doi:10.1186/s40645-020-00373-9.

cont'd. from pg. 1...

of an isothermal remanent magnetization (IRM) above 100 mT; the L-ratio; combinations of AF and thermal demagnetization and low-temperature measurements; and IRM component analysis.

These parameters mainly exploit the coercivity of hematite; while high coercivities can be attributed to either hematite or goethite, the focus is on hematite because it generally saturates magnetically near 3 T (Abrajevitch et al., 2018; Dunlop, 1971) as opposed to goethite, which only acquires 2–10% of its IRM below 3 T and remains unsaturated at 57 T (Rochette et al., 2005). This makes hematite more suitable than goethite for coercivity analysis in fields available in most laboratories. Some hematite samples can also require applied fields of 4.75 T to reach saturation (Bilardello, 2015; Bilardello & Kodama, 2009; Abrajevitch et al., 2018). This high saturation field exceeds the capability of most laboratory instruments, so capturing the full coercivity distribution for hematite is not always attainable. Hematite and goethite can also be distinguished from each other using high- and low-temperature measurements (e.g. Bilardello, 2019; France & Oldfield, 2000; Lagroix & Guyodo, 2017; Lowrie, 1990; Maher et al., 2004).

The key issue addressed by Roberts et al. (2020), however, is in distinguishing between high coercivity ("hard") and low coercivity ("soft") hematite, which are observed frequently in sediments, soils, and dust. Low and high coercivity hematite have been distinguished using detailed high temperature demagnetization (e.g. Bilardello, 2015; Swanson-Hysell et al., 2019), or chemical leaching (e.g. Bilardello & Kodama, 2010). However, the coercivity of soft hematite could overlap that of other soft phases such as magnetite/maghemite, which complicates coercivity analysis when quantifying magnetite/maghemite and hematite contributions. These observations constitute the crux of the issue discussed by Roberts et al. (2020), as reported on here.

The details

Details of hematite-related magnetic parameters are discussed in the IRMQ 27-4 article "Magnetic tests and characterization protocols: mineralogy and grain size / domain state Part I: isothermal strong field tests" by Volk et al. (2018) and by Roberts et al. (2020); they are not repeated here. However, the fundamental assumptions and requirements for use of these parameters are discussed here, as well as their limitations, following the outline of Roberts et al. (2020).

S-ratio: this parameter is based on the strong magnetic fields needed to saturate hematite compared to stoichiometric magnetite, which saturates below 300 mT, and the assumption that there is minimal overlap between their coercivity distributions. Typically, maximum fields of 1 or 1.5 T are used, so hematite likely remains unsaturated, and any contribution >300 mT is attributed to hematite and/or goethite, despite other minerals (e.g. oxidized phases, pyrrhotite) sometimes having coercivities >300 mT. Depending on the version of the S-ratio used, values range from -1 to 1 (Stober & Thompson, 1979), or from 0 to 1 (Bloemendal et al., 1992), which represent the range from high coercivity components only to low coercivity components only, respectively. Roberts et al. (2020), however, caution that extreme minimum (hard phase(s) only) values are not observed for either of the two S-ratios, even when magnetite comprises 0.05 wt% of the mixed sample (Fig. 1) because significant IRM acquisition also occurs below 300 mT in hematite samples (Fig. 2, and more below). Additionally, the maximum applied field used will affect how much of the hematite coercivity distribution is captured and reflected in the S-ratio value. In the examples shown in Fig. 1, maximum fields of 1 and 2 T were used, which are less than half of that required to saturate some hematite samples. Users should be aware that the S-ratio is highly non-linear; i.e., as the mass concentration of the high-coercivity mineral increases, the S-ratio does not decrease linearly owing to the contrasting spontaneous magnetizations of mag-

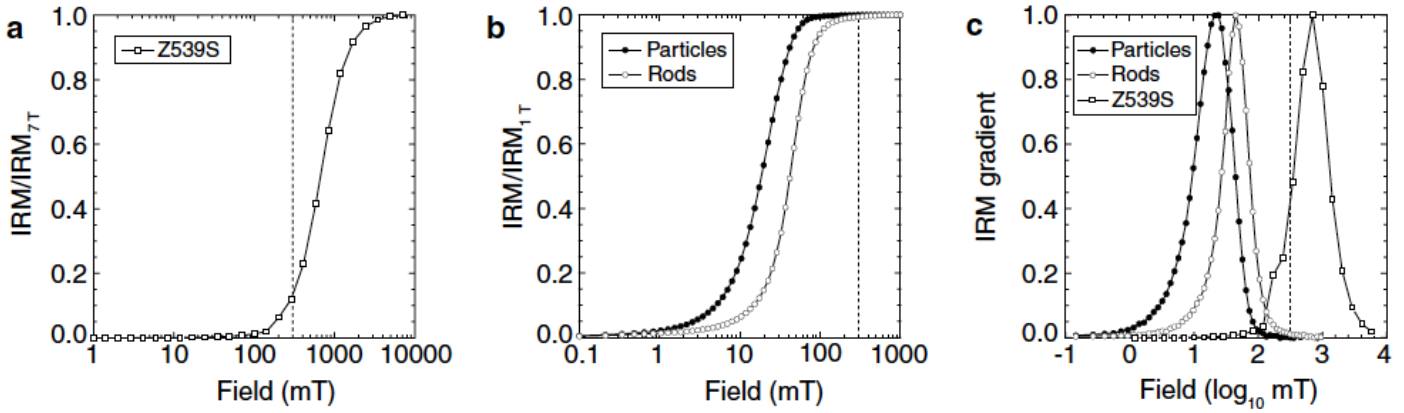

Figure 2. Illustration of IRM acquisition from Roberts et al. (2020): a) hematite; and b) magnetite. Small IRM acquisition below 300 mT in a) and complete acquisition of SIRM below 300 mT in b) explains the basis for use of a 300 mT cut-off field to discriminate between low-coercivity magnetite and high-coercivity hematite. The sample in a) is red pigmentary Zebra rock (Abrajevitch et al., 2018) and the samples in b) are synthetic nanomagnetites ("particles" are equidimensional magnetite (40–85 nm diameter); rods are elongated particles with length 250–300 nm and width 60–110 nm). c) First derivative curves of the IRM (i.e., gradient) for the three samples illustrated in a, b, which provide a measure of the respective coercivity distributions in relation to the 300 mT cut-off field. Dashed vertical lines represent the 300 mT cut-off field. Note the left-hand shoulder of the hematite gradient curve that extends below 300 mT.

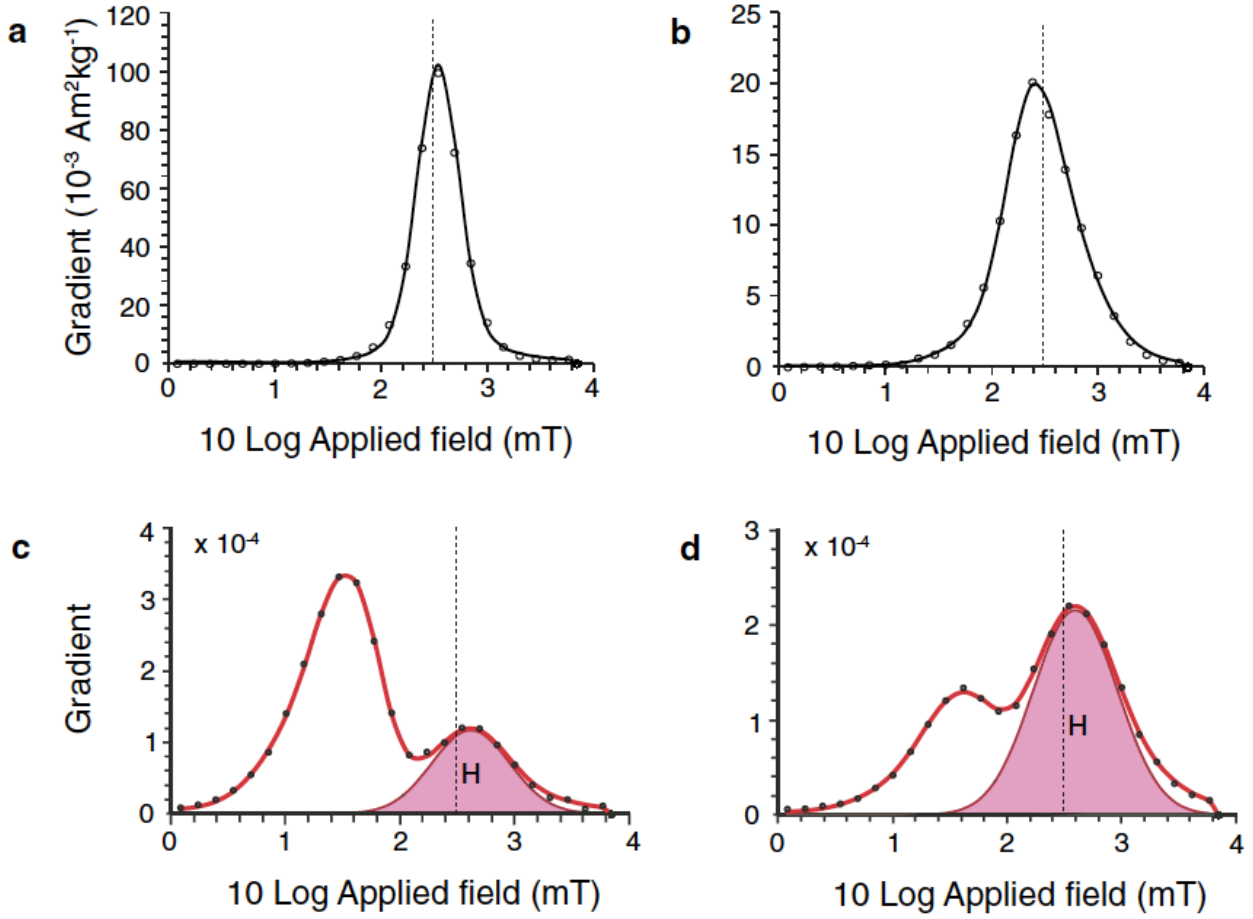

Figure 3. First derivative of IRM acquisition (gradient) curves and hematite components for 7 T maximum applied fields from Roberts et al. (2020). Results for hematite pigments in a decorative 'print stone' from the Mount McRae Shale Formation, Western Australia (Abrajevitch et al., 2014): a) hematite print stone pigment, and b) uniform pigment (see text for details). Results from Abrajevitch et al. (2015) for: c) Paleogene limestone 21 cm above the K–Pg boundary at Bottaccione Gorge, Italy, and d) limestone 46.5 cm below the boundary. For clarity, only the fitted hematite (labelled H) component of interest here is shown. Dashed vertical lines represent the 300 mT cut-off field.

netite (92 $Am^2 kg^{-1}$) and hematite (~0.4 $Am^2 kg^{-1}$) (Fig. 1) (Frank & Nowaczyk, 2008).

Hard-IRM (HIRM): this parameter (e.g. Robinson, 1986; Thompson & Oldfield, 1986) provides a measure of the absolute contribution of the high coercivity remanence contribution. As is the case for the S-ratio, a cut-off field is used, typically 300 mT. Any IRM acquisition above the cut-off is attributed to hematite and or goethite, and if both are present their contributions may be separated by demagnetizing above the Néel temperature of goethite (~120°C). This parameter has similar drawbacks as the S-ratio.

L-ratio: the L-ratio (Liu et al., 2007) builds from the S-ratio by providing a way to quantify the high coercivity mineral concentration (hematite, goethite). Here, a strong IRM, typically imparted in a 1 T field, is alternating field (AF)-demagnetized in a 100 mT field ($IRM_{AF100mT}$) and subsequently in a 300 mT field ($IRM_{AF300mT}$). In contrast to the S-ratio, the L-ratio ($IRM_{AF300mT}/IRM_{AF100mT}$, which can also be defined as $HIRM_{300mT}/HIRM_{100mT}$), exploits coercivity variations of hematite and goethite and allows targeting of specific coercivity distributions. Liu et al. (2007) further proposed that the AF values used may be modified to suit the coercivity distribution of studied samples (the L-ratio is, therefore, also independent of composition (cation-substitutions) on coercivity).

Variations and combinations of AF and thermal demagnetization: further parameters to characterize high coercivity mineral contributions, particularly when masked by strong magnetite contributions, include cyclic direct current (DC) demagnetization of the SIRM (Liu et al., 2002), AF-demagnetizing a SIRM at ~100 mT (Larrasoaña et al., 2003), and AF-demagnetizing at ~100 mT after each field application during an IRM acquisition experiment (Maher et al., 2004) to remove magnetite contributions. Bilardello and Kodama (2009) and Bilardello (2015) used the same approach in a double-IRM acquisition experiment to determine hematite saturation, in conjunction with heating to 125°C to remove the goethite contribution. Once saturation is reached, an AF + thermal demagnetization protocol was used in conjunction with chemical leaching by Bilardello and Kodama (2009) to separate pigmentary hematite of chemical origin from detrital hematite. Bilardello (2019) extended the HIRM test to low temperatures and incorporated the AF + thermal demagnetization approach as in the classic goethite test (Carter-Stiglitz et al., 2006; Guyodo et al.,

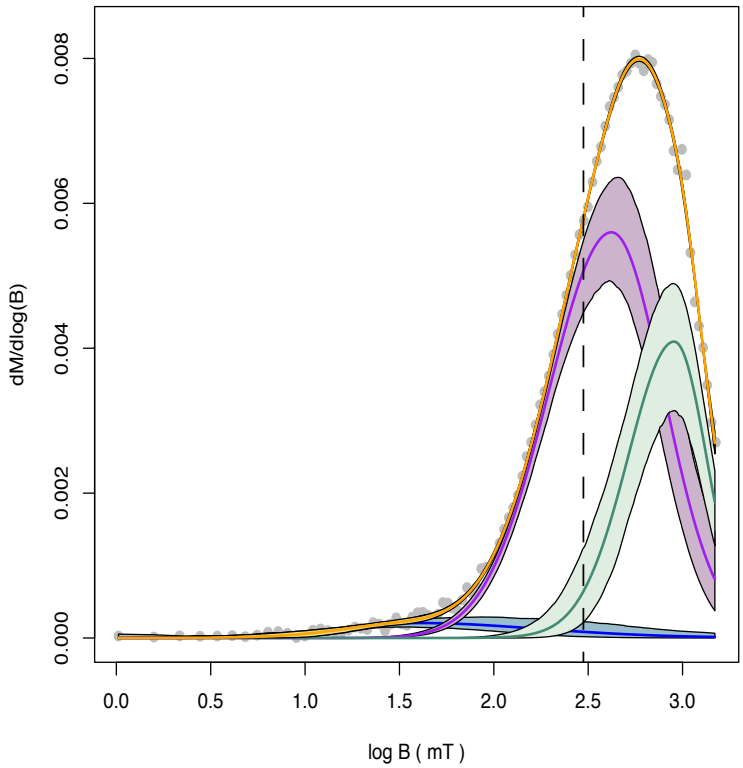

Figure 4. Unmixing of a Mauch Chunk Formation red bed sample from Pennsylvania (unpublished) from analysis of a backfield demagnetization curve in a 1.5 T maximum applied field. The specimen was determined to contain ~15-18% magnetite, 80-83% hematite (both detrital and pigmentary), and 1-3% goethite through application of the classic and HIRM goethite tests (Bilardello, 2019). While the goethite distribution is not apparent, likely due to its low relative abundance and the low maximum applied field, two hematite distributions are discernible and centered around 300-400 and 700-800 mT, consistent with pigmentary and detrital populations, respectively (e.g., Bilardello, 2015; Bilardello & Kodama, 2009, 2010; Swanson-Hysell et al., 2019).

2006). Measuring below room temperature (RT) allows quantification of contributions from finer particles with lower blocking temperatures, i.e. particles that are superparamagnetic (SP) at RT. The issue of soft hematite that unblocks above RT but demagnetizes in a few hundred mT, however, remains (more below).

IRM component analysis: magnetic components have continuous coercivity distributions, so component analysis of IRM acquisition and backfield demagnetization curves (generically referred to here as IRM acquisition curves) avoid the sharp cut-off at 300 mT or other fields. Fitting the first derivative of these curves allows coercivity contribution quantification (e.g. Egli, 2004; Heslop et al., 2002; Kruiver et al., 2001; Maxbauer et al., 2016b; Robertson & France, 1994), which deals more reasonably with inevitably overlapping component distributions. Hematite components will be evident in representations of the gradient of IRM acquisition curves (Fig. 2 c), especially if measurements are made to saturating fields or to non-saturating fields that are sufficient to define at least half of the coercivity distribution (if it is not skewed significantly).

Examples of hematite IRM components measured to 7 T by Abrajevitch et al. (2014, 2015) are illustrated in Fig. 3. Abrajevitch et al. (2014) showed that "non-uniformly" distributed pigmentary hematite (Fig. 3a) has a higher peak coercivity than a "uniformly distributed", pigment that contains appreciable goethite in addition to poorly crystalline hematite. (Fig. 3b). The distribution of the latter is broader and has a higher coercivity tail that requires high applied fields to reach saturation, which reflects the nature of the hematite nanocrystals in addition to goethite. The terms "uniform" and "non-uniform" here reflect the decimeter scale appearance of the pigmentary print-stones, with "non-uniform" referring to patchy orange-red coloration, not to grain size distributions. Importantly, both samples have significant coercivity distributions <300 mT.

Most natural samples contain multiple magnetic minerals, as illustrated in the bimodal coercivity distributions in Fig. 3c, d for limestone/shale interbeds (Abrajevitch et al., 2015) in which the pigmentary hematite contribution is highlighted. Like the pigmentary hematite illustrated in previous examples, a significant fraction of the fitted hematite coercivity distribution extends below 300 mT. These examples demonstrate that IRM component analysis is suitable for characterizing hematite components, particularly when large inducing fields are used. At typical maximum applied fields of 1 T, hematite components will still be well defined, although they will be truncated (Fig. 3), whereas any goethite distribution, if present, may not be resolved. Additionally, detrital and pigmentary hematite distributions within the same samples may be separated by coercivity spectra unmixing. The Mauch Chunk Formation, Pennsylvania, has remanence contributions from ~15-18% magnetite, 80-83% hematite (detrital and pigmentary), and 1-3% goethite based on the classic and HIRM goethite tests (Bilardello, 2019). Unmixing of backfield curves measured to 1.5 T maximum fields reveals that coercivity spectra can be fitted with a small but broad component centered at ~64 mT, which corresponds to magnetite and likely part of the finer hematite pigment. Two largely overlapping components centered at 379 and 784 mT (with associated uncertainties) make up the dominant peak, and likely correspond to softer and harder hematite contributions, respectively, although the latter distribution is truncated (Fig. 4). No distinct goethite peak, or shoulder, is discernible. These results agree with those of Swanson-Hysell et al. (2019) for Freda Formation red beds, which have two broad, overlapping populations centered at ~300 and 700 mT, respectively. From supporting rock-magnetic evidence and unblocking temperature modeling, they attributed the latter distribution to coarser single domain hematite, whereas the former corresponds to finer-grained hematite. The observed coercivity range corresponds to hematite grains smaller than 300 nm (e.g., Özdemir & Dunlop, 2014), which can have significant coercivity contributions <300 mT.

The explanation

While use of cut-off fields is convenient, it does not distinguish the true hematite component in the coercivity distributions shown above, and a large portion of the remanence extends below 300 mT for many hematite samples (Figs. 2, 3, and 5). Many natural soil and rock

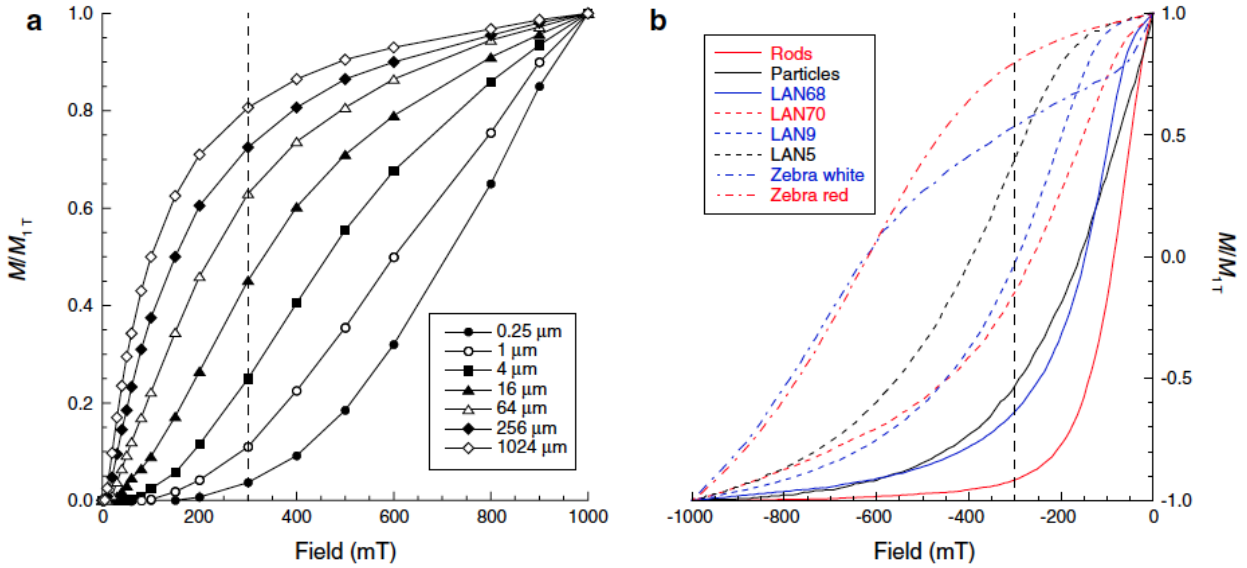

Figure 5. IRM acquisition and backfield demagnetization curves for hematite samples from Roberts et al. (2020). a) IRM acquisition curves for known hematite size fractions, where finer sizes are more resistant to acquisition (and vice versa). Redrawn from Thompson (1986). b) Backfield demagnetization curves for SD hematite samples (where DC demagnetization curves are equivalent to IRM acquisition curves with twice the amplitude and opposite slope for non-interacting SD particles). For sample details, see Roberts et al. (2020).

samples also have abundant hyperfine SP nanoparticle concentrations (e.g., Bilardello et al., 2020; Collinson, 1969; Creer, 1961; Swanson-Hysell et al., 2019). Hematite particle size distributions in such samples will likely span the magnetically unstable SP to stable SD size range (corresponding to 20-25 nm threshold size) for stoichiometric hematite (Banerjee, 1971; Özdemir & Dunlop, 2014), which will contribute a substantial low-coercivity distribution. Additionally, isomorphous cation substitution (e.g., Al^{3+} for Fe^{3+}) into the hematite lattice can lower the coercivity below 300 mT (Jiang et al., 2012). The SP/SD threshold size is ~17 nm for Al-substituted hematite (Jiang et al., 2014). Hematite particles below these threshold sizes are abundant in natural environments (e.g., Mehra & Jackson, 1960; Schwertmann, 1991), which is consistent with commonly observed magnetic viscosity in hematite (e.g., Collinson, 1969; Creer, 1961). Thus, low coercivity hematite will be important in many natural environments.

The coercivity of hematite particles increases with decreasing grain size from ~1 mm to ~250 nm (Thompson, 1986) (Fig. 5a), but, as shown above, it decreases for nanoparticles finer than ~250 nm that tend to be of greatest environmental and paleomagnetic importance. The significant hematite population below 300 mT is, thus, ignored when using a 300 mT cut-off field to calculate the S-ratio, HIRM, and other parameters, which will only reflect the highest coercivity hematite fraction. If goethite is not present, remanence acquisition above 300 mT is correctly attributed to hematite, but significant remanence acquisition from 0 to 300 mT (e.g., Figs. 3 and 5) will be attributed to other low-coercivity minerals. The S-ratio will, therefore, almost always under-estimate the relative hematite fraction, and HIRM will almost always under-estimate the absolute hematite concentration, both in favor of magnetite/maghemite. For example, for the 1 T maximum applied field used in Fig. 5a, S-ratio values vary up to 0.8 despite the fact that the samples contain no magnetite. S-ratio values up to +1 are illustrated in Fig. 6a for synthetic samples that contain only nanophase Al-substituted hematite or goethite (Liu et al., 2007). Also, owing to instrumental limitations, IRM acquisition experiments often involve measurement of hematite-bearing samples to maximum applied fields of 1 T. This will cause further underestimation of hematite contents when using the S-ratio or HIRM if a higher coercivity hematite component continues to acquire an IRM above 1 T, as in Figs. 3, 4, and 5. Routine hematite content underestimation with these magnetic methods deserves to be understood more widely. Use of such parameters could lead to significant misinterpretations, especially in quantitative environmental magnetic studies. To minimize such issues, Roberts et al. (2020) recommended combined use of magnetic and non-magnetic quantification methods.

Roberts et al. (2020) described three other issues related to the S-ratio. First, alternative formulations of the S-ratio with lower cut-off backfield values (e.g., 100 mT) are often used to assess magnetically soft components (e.g. Frank & Nowaczyk, 2008; Stober & Thompson, 1979; Stoner et al., 1996; Thompson & Oldfield, 1986). Users should be aware of the ambiguities inherent to such low-coercivity ranges, which are best used when magnetic assemblages are well constrained by other analyses. When the magnetic mineral assemblage under investigation is well understood, use of variable cut-off fields can be valuable. Second, Kruiver and Passier (2001) demonstrated that S-ratio values several percent below +1 can occur without addition of a high-coercivity mineral like hematite. S-ratio values < 1 can be due to coercivity hardening by surface oxidation of magnetite (e.g. Bilardello, 2020a; Cui et al., 1994; Kontny & Grothaus, 2017; Van Velzen & Dekkers, 1999; Van Velzen & Zijderveld, 1995). Third, when using the S-ratio, it should be noted that standard statistics, such as arithme-

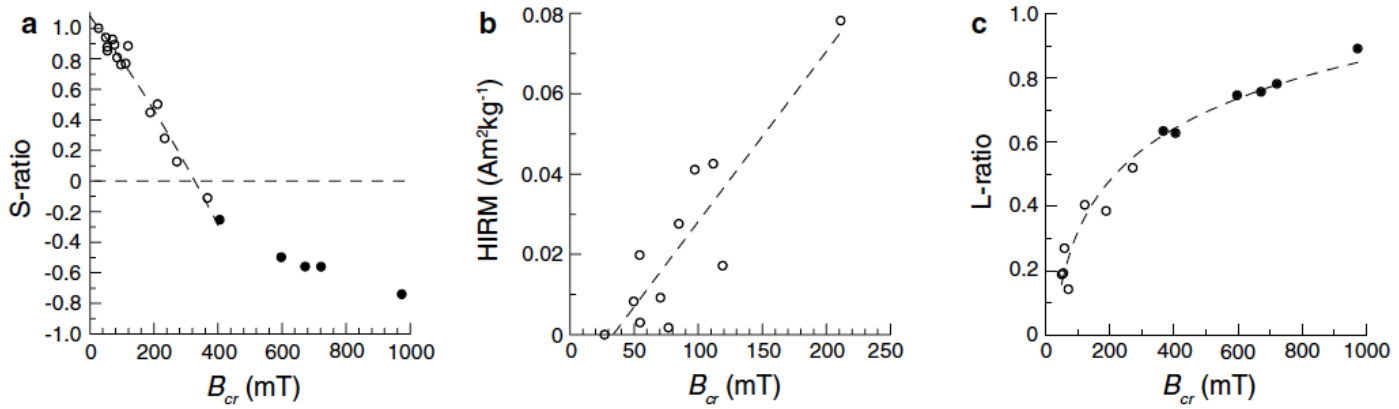

Figure 6. Coercivity variations and their influence on S-ratio and HIRM. a) S-ratio and b) HIRM versus coercivity of remanence (B_{cr}), where the S-ratio decreases with increasing coercivity and HIRM increases with increasing coercivity because more IRM is acquired above 300 mT as coercivity hardens. Such coercivity changes represent compositional differences in the analysed high-coercivity minerals, which can be assessed with c) the L-ratio. Constant L-ratio values indicate consistent magnetic properties of the high-coercivity component, and changing values represent variable coercivity. Open circles represent synthetic Al-substituted hematite and solid circles represent Al-substituted goethite (Redrawn by Roberts et al. (2020), without relationships for curve fits, from Liu et al. (2007)).

tic means and standard deviations, do not apply because the S-ratio provides relative, rather than absolute, information and is a bivariate measure represented by the low- and high-coercivity contributions that both lie in the range 0 to +1, that sum to one and are fundamentally interdependent (Heslop, 2009).

The highly variable coercivity of hematite (Figs. 3 and 5) means that the usefulness of simple parameters such as the S-ratio and HIRM will depend on the properties of hematite in a sample, which makes its quantification difficult. Such variations will be reflected in the L-ratio, which makes this proxy useful in scenarios with changing sediment source, cation substitution, particle size distribution, and varying hematite/goethite contents.

The Recommendation

IRM component analysis appears to be the most suitable of the methods discussed because it enables estimation of continuous, non-truncated coercivity distributions. If a hematite component is well defined, its magnitude can be calculated as a proportion of the total magnetization to allow hematite quantification even if magnetic saturation is not achieved. The 7 T maximum fields used in Fig. 3 capture the full hematite component, and a 4.75 T applied field will suffice for this purpose (Bilardello, 2015). Most studies use lower maximum applied fields, which need to be large enough to define the hematite component; fields up to 1.5 T can adequately define the hematite distribution if it is not skewed significantly. However, IRM curve analysis still has limitations for hematite quantification. Most studies provide evidence to identify whether a magnetic component is present or absent, which provides semi-supervised IRM unmixing that helps to reduce the non-uniqueness that is inherent to unmixing (Heslop, 2015). Nevertheless, the precise coercivity distribution of a magnetic component will remain unknown, as will its magnitude.

A useful "exercise" to ascertain the non-uniqueness of IRM unmixing, beyond the uncertainty of calculated fits, is to fit components to the same spectrum by starting from the lower coercivity end and then from the higher coercivity end. This will demonstrate the challenge of determining unique component fits to IRM acquisition curves; uncertainties associated with non-uniqueness of hematite component fits are, therefore, still likely to be significant. Therefore, substantial limitations exist for all existing magnetic proxies for hematite content. Additionally, room temperature remanence-based methods will not quantify ultrafine SP contents, which can be significant in hematite (e.g., Collinson, 1969; Creer, 1961). Although we lack simple ways to reliably quantify hematite contents in natural samples, the ambiguities that are inherent to hematite quantification can be reduced if proxies are used critically and in combination. For example, IRM component analysis can be used to check the coercivity range of hematite and the L-ratio can be used to check for variations in these ranges. If the L-ratio is variable, conventional use of the S-ratio and HIRM is unreasonable (Liu et al., 2007).

References

Abrajevitch, A., Pillans, B. J., & Roberts, A. P. (2014). Haematite pigmentation events and palaeomagnetic recording: implications from the Pilbara Print Stone, Western Australia. Geophysical Journal International, 199(2), 658–672. https://doi.org/10.1093/gji/ggu293

Abrajevitch, A., Font, E., Florindo, F., & Roberts, A. P. (2015). Asteroid impact vs. Deccan eruptions: the origin of low magnetic susceptibility beds below the Cretaceous–Paleogene boundary revisited. Earth and Planetary Science Letters, 430, 209–223. https://doi.org/10.1016/j.epsl.2015.08.022

Abrajevitch, A., Pillans, B. J., Roberts, A. P., & Kodama, K. (2018). Magnetic properties and paleomagnetism of Zebra Rock, Western Australia: chemical remanence acquisition in hematite pigment and Ediacaran geomagnetic field behavior. Geochemistry, Geophysics, Geosystems, 19(3), 732–748. https://doi.org/10.1002/2017GC007091

Banerjee, S. K. (1971). New grain size limits for palaeomagnetic stability in haematite. Nature Physical Science, 232, 15–16.

Bilardello, D. (2015). Isolating the anisotropy of the characteristic remanence-carrying hematite grains: a first multispecimen approach. Geophysical Journal International, 202(2), 695–712. https://doi.org/10.1093/gji/ggv171

Bilardello, D. (2019). Tinkering with the wheel: can the goe-

thite test run more smoothly? The IRM Quarterly, 29(2), 1–14.

Bilardello, D., & Kodama, K. P. (2009). Measuring remanence anisotropy of hematite in red beds: anisotropy of high-field isothermal remanence magnetization (hf-AIR). Geophysical Journal International, 178(3), 1260–1272. https://doi.org/10.1111/j.1365-246X.2009.04231.x

Bilardello, D., & Kodama, K. P. (2010). Palaeomagnetism and magnetic anisotropy of Carboniferous red beds from the Maritime Provinces of Canada: evidence for shallow palaeomagnetic inclinations and implications for North American apparent polar wander. Geophysical Journal International, 180(3), 1013–1029. https://doi.org/10.1111/j.1365-246X.2009.04457.x

Bilardello, D., Banerjee, S. K., Volk, M. W. R., Soltis, J. A., & Penn, R. L. (2020). Simulation of natural iron oxide alteration in soil: conversion of synthetic ferrihydrite to hematite without artificial dopants, observed with magnetic methods. Geochemistry, Geophysics, Geosystems, 21(7), 1–19. https://doi.org/10.1029/2020GC009037

Bilardello, D. (2020). Practical Magnetism II: humps and a bump, the maghemite song. The IRM Quarterly, 30(1), 1–17.

Bloemendal, J., King, J. W., Hall, F. R., & Doh, S. J. (1992). Rock magnetism of late Neogene and Pleistocene deep-sea sediments: relationship to sediment source, diagenetic processes, and sediment lithology. Journal of Geophysical Research, 97(B4), 4361–4375. https://doi.org/10.1029/91JB03068

Butler, R. F. (1992). Paleomagnetism: Magnetic Domains to Geologic Terranes. Boston: Blackwell.

Carter-Stiglitz, B., Valet, J. P., & LeGoff, M. (2006). Constraints on the acquisition of remanent magnetization in fine-grained sediments imposed by redeposition experiments. Earth and Planetary Science Letters, 245(1–2), 427–437. https://doi.org/10.1016/j.epsl.2006.03.002

Collinson, D. W. (1969). Investigations into the stable remanent magnetization of sediments. Geophysical Journal of the Royal Astronomical Society, 18(2), 211–222. https://doi.org/10.1111/j.1365-246X.1969.tb03563.x

Creer, K. M. (1961). Superparamagnetism in red sandstones. Geophysical Journal of the Royal Astronomical Society, 5(1), 16–28. https://doi.org/10.1111/j.1365-246X.1961.tb02925.x

Cui, Y., Verosub, K. L., & Roberts, A. P. (1994). The effect of low-temperature oxidation on large multi-domain magnetite. Geophysical Research Letters, 21(9), 757–760. https://doi.org/10.1029/94GL00639

Dekkers, M. J. (1990). Magnetic properties of natural goethite–III. Magnetic behaviour and properties of minerals originating from goethite dehydration during thermal demagnetization. Geophysical Journal International, 103(1), 233–250. https://doi.org/10.1111/j.1365-246X.1990.tb01765.x

Dunlop, D. J. (1971). Magnetic properties of fine-particle hematite. Annales de Géophysique, 27(3), 269–293. https://doi.org/10.1016/c2009-0-13025-8

Egli, R. (2004). Characterization of individual rock magnetic components by analysis of remanence curves, 1. unmixing natural sediments. Studia Geophysica et Geodaetica, 48(2), 391–446. https://doi.org/10.1023/B:SGEG.0000020839.45304.6d

France, D. E., & Oldfield, F. (2000). Identifying goethite and hematite from rock magnetic measurements of soils and sediments. Journal of Geophysical Research, 105(B2), 2781–2795.

Frank, U., & Nowaczyk, N. R. (2008). Mineral magnetic properties of artificial samples systematically mixed from haematite and magnetite. Geophysical Journal International, 175(2), 449–461. https://doi.org/10.1111/j.1365-246X.2008.03821.x

Guyodo Y., LaPara T. M., Anschutz A. J., Penn R. L., Banerjee S. K., Geiss C. E., & Zanner W. (2006). Rock magnetic, chemical and bacterial community analysis of a modern soil from Nebraska. Earth and Planetary Science Letters, 251, 168–178. https://doi.org/ 10.1016/j.epsl.2006.09.005.

Heller, F., & Liu, T. (1982). Magnetostratigraphical dating of loess deposits in China. Nature, 300, 431–433.

Heller, F., & Liu, T. (1984). Magnetism of Chinese loess deposits. Geophysical Journal of the Royal Astronomical Society, 77, 125–141.

Heslop, D. (2009). On the statistical analysis of the rock magnetic S-ratio. Geophysical Journal International, 178(1), 159–161. https://doi.org/10.1111/j.1365-246X.2009.04175.x

Heslop, D. (2015). Numerical strategies for magnetic mineral unmixing. Earth-Science Reviews, 150, 256–284. https://doi.org/10.1016/j.earscirev.2015.07.007

Heslop, D., Dekkers, M. J., Kruiver, P. P., & van Oorschot, I. H. M. (2002). Analysis of isothermal remanent magnetization acquisition curves using the expectation-maximization algorithm. Geophysical Journal International, 148, 58–64.

Jiang, Z. X., Liu, Q. S., Barrón, V., Torrent, J., & Yu, Y. J. (2012). Magnetic discrimination between Al-substituted hematites synthesized by hydrothermal and thermal dehydration methods and its geological significance. Journal of Geophysical Research: Solid Earth, 117(B2), n/a-n/a. https://doi.org/10.1029/2011JB008605

Jiang, Z. X., Liu, Q. S., Dekkers, M. J., Colombo, C., Yu, Y. J., Barron, V., & Torrent, J. (2014). Ferro and antiferromagnetism of ultrafine-grained hematite. Geochemistry, Geophysics, Geosystems, 15, 2699–2712. https://doi.org/10.1002/2014GC005377.

Kontny, A., & Grothaus, L. (2017). Effects of shock pressure and temperature on titanomagnetite from ICDP cores and target rocks of the El'gygytgyn impact structure, Russia. Studia Geophysica et Geodaetica, 61(1), 162–183. https://doi.org/10.1007/s11200-016-0819-3

Kruiver, P. P., Dekkers, M. J., & Heslop, D. (2001). Quantification of magnetic coercivity components by the analysis of acquisition curves of isothermal remanent magnetization. Earth and Planetary Science Letters, 189, 269–276.

Kruiver, P. P., & Passier, H. F. (2001). Coercivity analysis of magnetic phases in sapropel S1 related to variations in redox conditions, including an investigation of the S ratio. Geochemistry, Geophysics, Geosystems, 2(12), n/a-n/a. https://doi.org/10.1029/2001GC000181

Lagroix, F., & Guyodo, Y. (2017). A new tool for separating the magnetic mineralogy of complex mineral assemblages from low temperature magnetic behavior. Frontiers in Earth Science, 5, 1–11. https://doi.org/10.3389/feart.2017.00061

Larrasoaña, J. C., Roberts, A. P., Rohling, E. J., Winklhofer, M., & Wehausen, R. (2003). Three million years of monsoon variability over the northern Sahara. Climate Dynamics, 21(7–8), 689–698. https://doi.org/10.1007/s00382-003-0355-z

Liu, Q., Banerjee, S. K., Jackson, M. J., Zhu, R. X., & Pan, Y. X. (2002). A new method in mineral magnetism for the separation of weak antiferromagnetic signal from a strong ferrimagnetic background. Geophysical Research Letters, 29(12), 1565. https://doi.org/10.1029/2002GL014699

Liu, Q., Roberts, A. P., Torrent, J., Horng, C.-S., & Larrasoaña, J. C. (2007). What do the HIRM and S-ratio really measure in environmental magnetism? Geochemistry, Geophysics, Geosystems, 8(9), n/a-n/a. https://doi.org/10.1029/2007GC001717

Lowrie, W. (1990). Identification of ferromagnetic minerals in a rock by coercivity and unblocking temperature properties, Geophysical Research Letters, 17(2), 159–162.

Maher, B. A., Karloukovski, V. V., & Mutch, T. J. (2004). High-field remanence properties of synthetic and natural submicrometre haematites and goethites: significance for environmental contexts. Earth and Planetary Science Letters, 226(3–4), 491–505. https://doi.org/10.1016/j.epsl.2004.05.042

Maxbauer, D. P., Feinberg, J. M., & Fox, D. L. (2016a). Magnetic mineral assemblages in soils and paleosols as the basis for paleoprecipitation proxies: a review of magnetic methods and challenges. Earth-Science Reviews, 155, 28–48. https://doi.org/10.1016/j.earscirev.2016.01.014

Maxbauer, D. P., Feinberg, J. M., & Fox, D. L. (2016b). MAX UnMix: a web application for unmixing magnetic coercivity distributions. Computers and Geosciences, 95, 140–145. https://doi.org/10.1016/j.cageo.2016.07.009

Mehra, B. A., & Jackson, M. L. (1960). Iron oxide removal from soils and clays by a dithionite-citrate system buffered with sodium bicarbonate. Clays and Clay Minerals, 7, 317–327.

Özdemir, Ö., & Dunlop, D. J. (2014). Hysteresis and coercivity of hematite. Journal of Geophysical Research: Solid Earth, 119(4), 2582–2594. https://doi.org/10.1002/2013JB010739

Roberts, A. P., Zhao, X., Heslop, D., Abrajevitch, A., Chen, Y. H., Hu, P., et al. (2020). Hematite (α-Fe_2O_3) quantification in sedimentary magnetism: limitations of existing proxies and ways forward. Geoscience Letters, 7, 8. https://doi.org/10.1186/s40562-020-00157-5

Robertson, D. J., & France, D. E. (1994). Discrimination of remanence carrying minerals in mixtures, using isothermal remanent magnetization aquisition curves. Physics of the Earth and Planetary Interiors, 82, 223–234.

Robinson, S. G. (1986). The late Pleistocene palaeoclimatic record of North Atlantic deep-sea sediments revealed by mineral-magnetic measurements. Physics of the Earth and Planetary Interiors, 42(1–2), 22–47. https://doi.org/10.1016/S0031-9201(86)80006-1

Rochette, P., Mathé, P. E., Esteban, L., Rakoto, H., Bouchez, J. L., Liu, Q., & Torrent, J. (2005). Non-saturation of the defect moment of goethite and fine-grained hematite up to 57 Teslas. Geophysical Research Letters, 32(22), 1–4. https://doi.org/10.1029/2005GL024196

Schwertmann, U. (1985). The effect of pedogenic environments on iron oxide minerals. Advances in Soil Science, 1, 171–200.

Schwertmann, U. (1991). Solubility and dissolution of iron oxides. Plant and Soil, 130(1–2), 1–25. https://doi.org/10.1007/BF00011851

Stober, J. C., & Thompson, R. (1979). An investigation into the source of magnetic minerals in some Finnish lake sediments. Earth and Planetary Science Letters, 45, 464–474.

Stoner, J. S., Channell, J. E. T., & Hillaire-Marcel, C. (1996). The magnetic signature of rapidly deposited detrital layers from the deep Labrador Sea: relationship to North Atlantic Heinrich layers. Paleoceanography, 11(3), 309–325. https://doi.org/10.1029/96PA00583

Swanson-Hysell, N. L., Fairchild, L. M., & Slotznick, S. P. (2019). Primary and secondary red bed magnetization constrained by fluvial intraclasts. Journal of Geophysical Research: Solid Earth, 124(5), 4276–4289. https://doi.org/10.1029/2018JB017067

Thompson, R. (1986). Modelling magnetization data using SIMPLEX. Physics of the Earth and Planetary Interiors, 42(1–2), 113–127. https://doi.org/10.1016/S0031-9201(86)80013-9

Thompson, R., & Oldfield, F. (1986). Environmental Magnetism. Allen and Unwin.

Van Velzen, A. J., & Dekkers, M. J. (1999). Low-temperature oxidation of magnetite in loess-paleosol sequences: a correction of rock magnetic parameters. Studia Geophysica et Geodaetica, 43(4), 357–375. https://doi.org/10.1023/A:1023278901491

Van Velzen, A. J., & Zijderveld, J. D. A. (1995). Effects of weathering on single-domain magnetite in Early Pliocene marine marls. Geophysical Journal International, 121, 267–278.

Volk, M. W. R., Jackson, M. J., & Bilardello, D. (2018). Magnetic tests and characterization protocols: mineralogy and grain size / domain state Part I: isothermal strong field tests. The IRM Quarterly, 27(4), 1–21.

RAC News

Julie Bowles (University of Wisconsin, Milwaukee) is the new chair of the IRM's Research Advisory Committee.

Thank you Julie for accepting this position!

University of Minnesota
John T. Tate Hall, Room 150
116 Church Street SE
Minneapolis, MN 55455-0149
phone: (612) 624-5274
e-mail: irm@umn.edu
www.irm.umn.edu

Nonprofit Org.
U.S Postage
PAID
Twin Cities, MN
Permit No. 90155

The IRM Quarterly

The *Institute for Rock Magnetism* is dedicated to providing state-of-the-art facilities and technical expertise free of charge to any interested researcher who applies and is accepted as a Visiting Fellow. Short proposals are accepted semi-annually in spring and fall for work to be done in a 10-day period during the following half year. Shorter, less formal visits are arranged on an individual basis through the Facilities Manager.

The *IRM* staff consists of **Subir Banerjee**, Professor/Founding Director; **Bruce Moskowitz**, Professor/Director; **Joshua Feinberg**, Assistant Professor/Associate Director; **Maxwell Brown, Peat Sølheid** and **Dario Bilardello**, Staff Scientists.

Funding for the *IRM* is provided by the **National Science Foundation**, the **W. M. Keck Foundation**, and the **University of Minnesota**.

The *IRM Quarterly* is published four times a year by the staff of the *IRM*. If you or someone you know would like to be on our mailing list, if you have something you would like to contribute (*e.g.*, titles plus abstracts of papers in press), or if you have any suggestions to improve the newsletter, please notify the editor:

Dario Bilardello
Institute for Rock Magnetism
University of Minnesota
150 John T Tate Hall
116 Church Street SE
Minneapolis, MN 55455-0128
phone: (612) 624-5049
e-mail: dario@umn.edu
www.irm.umn.edu

UNIVERSITY OF MINNESOTA